



ANALYSIS OF VIBRATION CHARACTERISTICS IN ROLLING BEARING ROTOR SYSTEMS: CONSIDERING RADIAL CLEARANCE AND OUTER RACEWAY DEFECTS

¹Mr.M.Hari Prasad,²Mr.R.pandu,³Mr.S.Naresh,⁴Mrs M.Swarna

¹²³⁴Assistant Professor

Department of Mechanical Engineering

Samskruti College of Engineering and Technology, Hyderabad

ABSTRACT:

The radial clearance of a rolling bearing causes its radial stiffness to exhibit time-varying characteristics, which may result in a measurable vibration. Inadequate lubrication may induce vibration, which in turn may produce tiny flaws on the raceway of the rolling bearing. In this research, we build a dynamic model of the rolling bearing rotor system that accounts for the radial clearance and outer raceway defect. Rolling bearings' time-dependent stiffness is modelled using a substitution of 8th-order Fourier series. In order to examine the fault characteristic frequency of rolling bearing, we must first get the vibration response of the rotor system. By analysing the vibration signal's frequency spectrum, we may determine the defect characteristic frequency of the test bearing during a rolling bearing rotor system vibration test. Good agreement between experimental and theoretical data confirms the accuracy of the dynamic model.

11099

Vibration characteristics, outer raceway defect, bearing rotor system, time-varying stiffness, and rolling bearings are some examples of keywords.

DOI Number: 10.48047/nq.2022.20.8.nq221144

NeuroQuantology 2022; 20(8): 11099-11109

I.INTRODUCTION:

With the advantages of low frictional resistance and high rotation accuracy, the rolling bearing has been widely used in rotating machinery, such as machine tools, aerospace equipment, electronics, and precision instruments.1–3 The stiffness of rolling bearing is regarded as a significant factor affecting the dynamic characteristics of bearing rotor system. Due to the existence of the rolling elements, the stiffness of rolling bearing shows obvious time-varying characteristics.4–6 Stribeck7 deduced

the maximum load contact formula of the rolling element by analyzing the working state with the rolling element at the bottom. Perretet al.8 found that the load distribution, contact area, and contact stress were changed with time caused by the rotation of the rolling element in engineering practice. These cases resulted in the changes of stiffness with time,9–11 and induced nonlinear vibration and instability of rolling bearing rotor system finally.12–15 Cao et al.16 researched the stiffness variation



rules of rolling bearing under the static load and unbalanced load

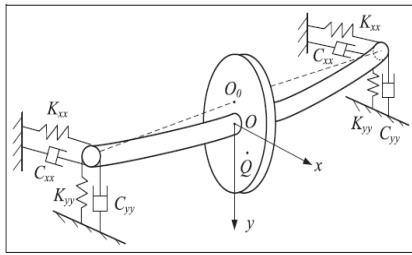


Figure 1. Dynamical model of bearing rotor system.

excitation, and calculated the vibration response of time domain and the frequency domain characteristics of the rotor under the time-varying bearing stiffness. Liu and Zhang¹⁷ deduced the time-varying stiffness of rolling bearings under different combined load sets by the implicating function derivation.

The vibration and shock of the bearing rotor system is caused by the time-varying characteristic of rolling bearing stiffness, which aggravates the generation of small defects on the raceway. Cheng et al.¹⁸ established a quasi-static analysis model of rolling bearing with local defects by introducing the local contour functions such as the depth and circumferential variation of local into the analysis model. Petersen et al.¹⁹ established a contact stiffness model of bearing related to the defect size based on the internal load distribution of rolling bearings with defects in the outer ring. Cui et al.²⁰ simulated the vibration response signals of rolling bearings under different fault sizes by introducing the outer ring defect size parameters into the dynamic model. Jiang et al.²¹ improved the dynamic model with three-dimensional geometric defect regions by extending the geometric parameters of the outer raceway defect regions. Singh et al.²² solved the bearing FEM model with outer raceway defect by LS-DYNA, and analyzed the simulation results. Zhao et al.²³ researched the effects of defect size, position, and number on bearing dynamic behaviors are investigated with the aid of phase trajectories, shaft center orbits, FFT spectra, etc. Tang et al.²⁴ analyzed

the load of rolling elements passing through the defect area under different conditions based on Gupta model. Ma et al.²⁵ added the three different types of bearing defects into the defect model considering the force transfer between the vehicle and the bearing. Lu et al.²⁶ proposed the defect modeling algorithm of inner raceway, outer raceway and rolling element, and obtained the theoretical rolling track when the rolling element passes through the defect position. These studies only consider the defects of rolling bearings, but don't consider the time-varying characteristics of bearing stiffness.

The dynamic model of rolling bearing rotor system considering the radial clearance and outer raceway defect is established for the spindle bearings of machine tool in this paper. The time-varying stiffness of bearing is fitted, and the vibration response of rolling bearing rotor system is analyzed. The fault characteristic frequency of rolling bearing identified by the vibration response is compared with the experiment results.

Dynamical modeling of rolling bearing rotor system

Dynamical model of rotor system

For the rolling bearing rotor system, the rotor is supported by two identical rolling bearings at both ends, and the external load is applied at the middle position. The bearing can be simplified as an isotropic spring-damp system assuming that the bearing is supported rigidly.²⁷ The stiffness and damping coefficients in the horizontal direction are k_{xx} and c_{xx} respectively, and in the vertical direction are k_{yy} and c_{yy} respectively.

The dynamical model of the bearing rotor system is shown in Figure 1. O_0 is the center of the static balance of the rotor. When the rotor rotates, the unbalanced force causes the axis to deviate from the static balance position. At this time, the center of rotor is O , which is the original point of coordinate system xOy .

According to the principle of force balance, the differential equations of motion of rolling bearing rotor system are:

$$\begin{cases} M \cdot \ddot{x} + C \cdot \dot{x} + K_x \cdot x = F_0 \cdot \sin(\omega \cdot t) \\ M \cdot \ddot{y} + C \cdot \dot{y} + K_y \cdot y = F + F_0 \cdot \cos(\omega \cdot t) + M \cdot g \end{cases} \quad (1)$$

Where M is the mass of bearing-rotor system. C is the supporting damping coefficient of bearing-rotor system, which is the contact damping of rolling bearing. K_x, K_y are the equivalent stiffness of the rolling bearing rotor system in the horizontal and vertical directions, $K_x = k_{kxx}/(k + k_{xx}), K_y = k_{kyy}/(k + k_{yy})$, k is the rotor bending stiffness, $k = 12pER^4/L^3$. E is the elastic modulus. R is the journal radius. L is the distance between the center of two bearings. v is the angular speed of the rotor. F_0 is the centrifugal force caused by the unbalanced mass of the rotor. g is the gravitational acceleration. F is the external exciting force.

Rolling bearing stiffness model with outer raceway defects

Defect model on outer raceway. It is supposed that there is a rectangular notch on the outer raceway ring, the defect depth is H_b , the defect length is L_b , the corresponding wrap angle is θ_b , the diameter of the rolling

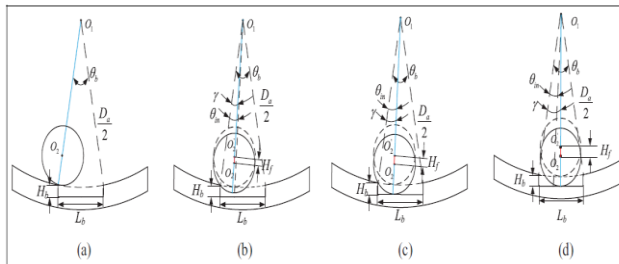


Figure 2. Additional displacement of rolling elements passing through defect of outer raceway: (a) $\gamma = 0$, (b) $0 < \gamma < \theta_{in}$, (c) $\gamma = \theta_{in}$, and (d) $\theta_{in} < \gamma < \theta_b - \theta_{in}$.

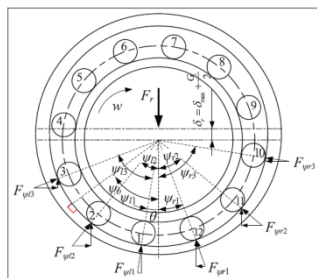


Figure 3. Force analysis of rolling bearing with radial clearance.

element is D_w , and the diameter of the outer raceway of the bearing is D_a . From the rolling element enters the defect to leaves the defect, H_f is the additional displacement of the rolling element, and g is the angle between the center of rolling element and the starting position of the defect. For the large outer raceway defect ($D_w \setminus L_b$), when the rolling element begins to enter the outer raceway defect ($g=0$), the additional displacement is 0 (as shown in Figure 2(a)). When the rolling element passes through the bottom of outer raceway defect ($\theta_{in} \leq g \leq \theta_b$), the additional displacement is the maximum value at this time, which is equal to the defect depth of the outer raceway (as shown in Figure 2(d)). When the rolling element is entering or leaving the defect ($0 < g < \theta_{in}$ or $\theta_b - \theta_{in} < g < \theta_b$), it only contacts with one side of the defect (as shown in Figure 2(b)). In order to analyze the additional displacement of the rolling element during the rolling element passage through the outer raceway defect, the change of the additional displacement is simplified as the linear change, and the defect is assumed to be a smooth surface. The wrap angle between the starting point of the outer ring defect area and the point of the maximum additional displacement θ_{in} is proposed to calculate the additional displacement H_f , which can be expressed as follows:

$$\theta_{in} \approx \arcsin \left(\sqrt{\left(\frac{D_w}{2}\right)^2 - \left(\frac{D_w}{2} - H_b\right)^2} / \frac{D_a}{2} \right) \quad (2)$$

When the rolling element passes through the outer raceway defect position, the additional displacement of the rolling element H_f can be expressed as:

$$H_f = \begin{cases} \frac{H_b \gamma}{\theta_{in}}, & 0 < \gamma < \theta_{in} \\ H_b, & \theta_{in} \leq \gamma \leq \theta_b - \theta_{in} \\ \frac{H_b}{\theta_{in}} (\theta_b - \gamma), & \theta_b - \theta_{in} < \gamma < \theta_b \\ 0, & \text{another} \end{cases} \quad (3)$$

The similar method can be used to analyze the small outer raceway defect ($D_w \leq L_b$), which is

not be described because of the length of this paper.

Stiffness model of rolling bearing. The defects could exist anywhere in the outer raceway, the outer raceway can be divided into loading area and non-loading area according to the load distribution (as shown in Figure 3). When the defect of the outer raceway is in the non-loading area, there is almost no impact on the dynamic characteristics of the bearing because the rolling element does not contact with the track of rolling bearing. Therefore, the defect of the outer raceway in the loading area is analyzed.

The force analysis of rolling bearing with radial clearance is shown in Figure 3. ψ is the rotation position angle of the rolling element. ω is the angular velocity of the rolling bearing. ψ_b is the angle between the left rolling elements and the bearing axis in the vertical direction. ψ_r is the angle between the right rolling elements and the bearing axis in the vertical direction. When the rolling element passes through the defect of the rolling bearing without radial clearance, the additional displacement will result in the change of load distribution and local elastic deformation. The elastic deformation of the rolling element along the Hertz contact normal line can be expressed as:

$$\delta_{\psi_b} = \delta_{\max} \cos \psi_b - H_f \quad (4)$$

Where δ_{ψ_b} is the elastic deformation of the rolling element at the defect, δ_{\max} is the maximum elastic deformation of the elastomer.

The load of the rolling element at the defect F_{ψ_b} is:

$$F_{\psi_b} = F_{\max} \left(\frac{\delta_{\psi_b}}{\delta_{\max}} \right)^{1.5} = F_{\max} \left(\cos \psi_b - \frac{H_f}{\delta_{\max}} \right)^{1.5} \quad (5)$$

Where F_{\max} is the maximum load of the rolling element. According to the principle of force balance, the

radial load of rolling bearing should be equal to the resultant force of each rolling element in the vertical direction:

$$F_r = F_{\max} \left[\sum_{i=1}^n \cos^{2.5}(\psi_i + \omega t) + \left(\cos \psi_b - \frac{H_f}{\delta_{\max}} \right)^{1.5} \cos \psi_b \right] \quad (6)$$

Where F_r is the radial external load of the rolling bearing.

The maximum load of the rolling element can be expressed as:

$$F_{\max} = \frac{F_r}{\left[\sum_{i=1}^n \cos^{2.5}(\psi_i + \omega t) + \left(\cos \psi_b - \frac{H_f}{\delta_{\max}} \right)^{1.5} \cos \psi_b \right]} \quad (7)$$

11102

The load distribution of each rolling element of rolling bearing without radial clearance can be expressed as:

$$F_{\psi_i} = \frac{F_r \cos^{1.5} \psi_i}{\left[\sum_{i=1}^n \cos^{2.5}(\psi_i + \omega t) + \left(\cos \psi_b - \frac{H_f}{\delta_{\max}} \right)^{1.5} \cos \psi_b \right]} \quad (8)$$

When the rolling element passes through the defect of bearing with radial clearance, the elastic deformation of the rolling element along the Hertz contact normal line can be expressed as:

$$\delta_{\psi_b} = \left(\delta_{\max} + \frac{G_r}{2} \right) \cos \psi_b - \frac{G_r}{2} - H_f \quad (9)$$

Where G_r is the radial clearance of bearing. The load of the rolling element at the defect can be obtained from the derivation of the above formula for the load distribution on each rolling element of the rolling bearing without radial clearance, which can be expressed as:

$$\begin{aligned} F_{\psi_b} &= F_{\max} \left(\frac{\delta_{\psi_b}}{\delta_{\max}} \right)^{1.5} \\ &= F_{\max} \left(\frac{(\delta_{\max} + G_r/2) \cos \psi_b - G_r/2 - H_f}{\delta_{\max}} \right)^{1.5} \end{aligned} \quad (10)$$

The load distribution coefficient T is proposed to simplify the maximum load F_{\max} of rolling element of rolling bearing with radial clearance.

Define $T=(12Gr/(2d_{max} + Gr))/2$, so the F_{cb} can be expressed as:

$$F_{\psi_b} = F_{max} \left(\frac{\cos \psi_b}{2T} - \frac{G_r/2 + H_f}{\delta_{max}} \right)^{1.5} \quad (11)$$

The iteration process of solving F_{max} is shown in Figure 4. Therefore, the maximum load of the rolling bearing with the radial clearance F_{max} at the n th iteration can be expressed:

$$F_{max}^n = \frac{F_r}{\left(\sum_{i=1}^m \left(\frac{\delta_r^n \cos \psi_i - G_r/2}{\delta_{max}^n} \right)^{1.5} \cos \psi_i + \left(\frac{\delta_r^n \cos \psi_b - G_r/2 - H_f}{\delta_{max}^n} \right)^{1.5} \cos \psi_b \right)} = \frac{\sum_{i=1}^m F_{\psi_i} \cos \psi_i + F_{\psi_b} \cos \psi_b}{\left(\sum_{i=1}^m \left(\frac{\delta_r^n \cos \psi_i - G_r/2}{\delta_{max}^n} \right)^{1.5} \cos \psi_i + \left(\frac{\delta_r^n \cos \psi_b - G_r/2 - H_f}{\delta_{max}^n} \right)^{1.5} \cos \psi_b \right)} \quad (12)$$

The rolling bearing can be simplified as the mass system with many elastic elements connection, as show in Figure 5. The outer ring of bearing is fixed to the bearing seat and the inner ring is linked to the spindle. The contact deformation between the roller element and the outer ring can be regarded as the spring compression under the radial external force. Therefore, the stiffness of rolling bearing under the radial external load can be expressed as:

$$K = \frac{F}{\delta} \quad (13)$$

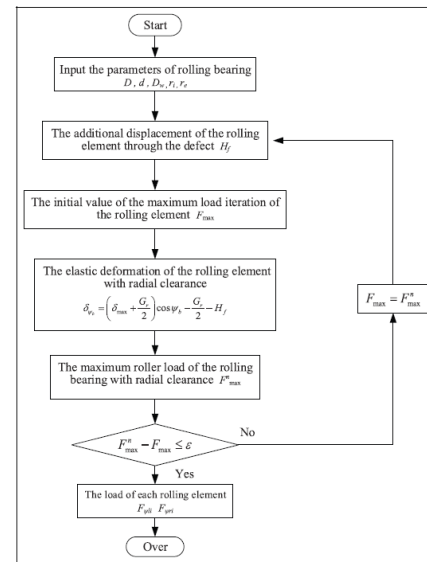


Figure 4. Iterative calculation process.

When $F_{max}^n - F_{max}^{n-1} \leq \epsilon$, the iteration finishes, the stiffness of rolling bearing with the outer raceway defect under the radial external load can be expressed as:

$$K = \sum_{li=0}^{nl} \left(\frac{\partial F_{\psi_{li}}}{\partial \delta_{\psi_{li}}} \cdot \cos^2 \psi_{li} \right) + \sum_{ri=0}^{nr} \left(\frac{\partial F_{\psi_{ri}}}{\partial \delta_{\psi_{ri}}} \cdot \cos^2 \psi_{ri} \right) \quad (14)$$

Where d_{cli} is the contact normal elastic deformation of the rolling element on the left side, $li=1, 2, \dots, nl$.

F_{cli} is the contact normal force of the rolling element on the left side, $li=1, 2, \dots, nl$. d_{cri} is the contact normal elastic deformation of the rolling element on the right side, $ri=1, 2, \dots, nr$. F_{cri} is the contact normal force of the rolling element on the right side, $ri=1, 2, \dots, nr$.

Time-varying stiffness analysis of rolling bearings

Taking the deep groove ball bearing 6206 as an example, the defect length L_b is 2mm, the depth H_b is 1.5mm, and the defect position angle is 0° . The structural parameters and working conditions of the rotor

and bearing are shown in Tables 1 and 2 Based on the rolling bearing stiffness



model considering the outer raceway defect, the time-varying

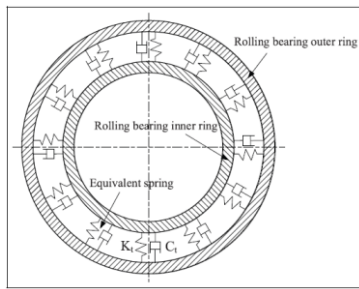


Figure 5. Siffness model of rolling bearing.

stiffness of the defective bearing is calculated. The bearing stiffness changing with time shows periodic changes in both horizontal and vertical directions, so it can be fitted as a trigonometric series by Fourier expansion. The stiffness variation curve of the defective bearing in the horizontal and vertical directions is fitted by the MATLAB software. The fitting results of the 8-order Fourier expansions of the bearing stiffness are shown in Figures 6 and 7. The determination coefficients of each order of fitting results (R-squared) are shown in Table 3. It can be seen from Figure 6 and Table 3 that the horizontal bearing stiffness changing with time is well fitted with the 8-order Fourier series expansion curve. The determination coefficient R-square of the fitting result is 0.9907. From Figure 7 and Table 3, the stiffness in the vertical direction of the bearing changing with time fits well with the 7-order Fourier series expansion curve, and the determination coefficient R-square is 0.9926. The fitting accuracy can both meet the calculation requirements. Therefore, the time-varying stiffness function expressions of the bearing in the horizontal and vertical directions are:

$$K_x(t) = a_{x0} + \sum_{xi=1}^8 (a_{xi} \cos(xi \cdot \omega \cdot t) + b_{xi} \sin(xi \cdot \omega \cdot t)) \tag{15}$$

$$K_y(t) = a_{y0} + \sum_{yi=1}^7 (a_{yi} \cos(yi \cdot \omega \cdot t) + b_{yi} \sin(yi \cdot \omega \cdot t)) \tag{16}$$

The coefficients of the Fourier expansion in the horizontal and vertical directions are shown in Table 4 according to equations (15) and (16).

Table 1. Parameters of deep groove ball bearing 6206.

Parameter	Value	Parameter	Value
Bearing outside diameter D/mm	62	Radius of curvature of inner raceway r _i /mm	4.91
Bearing bore diameter d/mm	30	Radius of curvature of outer raceway r _o /mm	5.00
Bearing width B/mm	16	Inner raceway diameter d _i /mm	36.97
Roller diameter D _r /mm	9.53	Outer raceway diameter D _o /mm	56.03
Pitch diameter D _p /mm	46.5	Sum of inner raceway curvature Σρ _i /mm	0.2701
Quality of bearing m/kg	0.20	Sum of outer raceway curvature Σρ _o /mm	0.1842
Number of rolling elements Z	9	Difference of curvature of inner raceway F(ρ _i)/mm	0.9547
Radial load F _r /N	600	Difference of curvature of outer raceway F(ρ _o)/mm	0.8915

Table 2. Structure parameters of rotor.

Parameter	Value	Parameter	Value
Length L _{rot} /mm	278	Rotor material	Q235
Quality M _{rot} /kg	1.967	Poisson ratio ν	0.28
Quality and grade of balance G	1	Density ρ/kg·m ⁻³	7800
Rotation speed n/r·min ⁻¹	1500	Modulus of elasticity E/Pa	2.1 × 10 ¹¹
Distance between supporting points L/mm	210	/	/

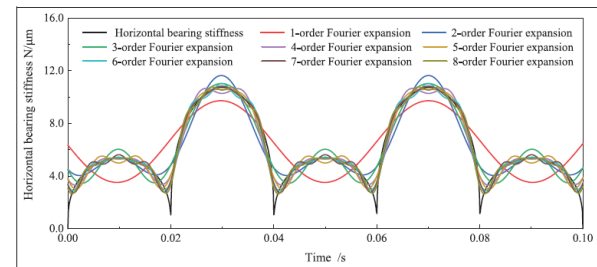


Figure 6. Time-varying stiffness in the horizontal direction.

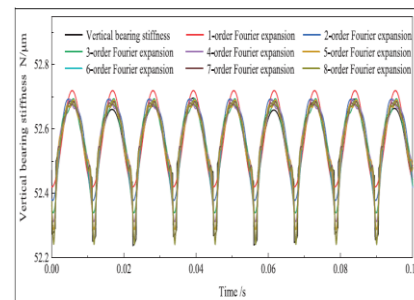


Figure 7. Time-varying stiffness in the vertical direction.

Table 3. Value of R-squared.

Order	1-order	2-order	3-order	4-order	5-order	6-order	7-order	8-order
R-square								
Horizontal direction	0.6462	0.8902	0.9154	0.9524	0.9587	0.9715	0.9801	0.9907
Vertical direction	0.9674	0.9740	0.9744	0.9849	0.9849	0.9849	0.9926	0.9926

Table 4. Fourier expansion coefficients.

Coefficients of horizontal Fourier expansion				Coefficient of vertical Fourier expansion			
Coefficient	Value	Coefficient	Value	Coefficient	Value	Coefficient	Value
a_0	6.616×10^6	b_1	1	a_0	5.256×10^7	b_1	1
a_1	-5.891×10^4	b_2	-3.11×10^6	a_1	-1.487×10^5	b_2	-9658
a_2	-1.916×10^6	b_3	5.539×10^4	a_2	-3.757×10^4	b_3	-2.021×10^4
a_3	-3.184×10^4	b_4	-6.184×10^3	a_3	-1.645×10^4	b_4	-2.628×10^4
a_4	-7.474×10^5	b_5	4.014×10^3	a_4	-7665	b_5	-2.772×10^4
a_5	-2.84×10^4	b_6	-3.083×10^3	a_5	176.4	b_6	-2.503×10^4
a_6	-4.373×10^5	b_7	3.742×10^4	a_6	6664	b_7	-1.941×10^4
a_7	-2.409×10^4	b_8	-1.938×10^3	a_7	9799	b_8	-1.256×10^4
a_8	-3.004×10^5	b_9	3.416×10^4	a_8	1	b_9	1

Vibration response analysis of rolling bearing rotor system

The time-varying stiffness fitting function of the bearing with outer raceway defects is substituted into equation (1), and the differential equation of motion of the rotor system considering the time-varying stiffness of the bearing and the raceway defects is as follow:

$$\begin{aligned}
 M\ddot{x} + C\dot{x} + \left(a_{x0} + \sum_{xi=1}^8 (a_{xi}\cos(xi \cdot \omega_x \cdot t) + b_{xi}\sin(xi \cdot \omega_x \cdot t)) \right) x \\
 = F_0 \sin(\omega \cdot t) \\
 M\ddot{y} + C\dot{y} + \left(a_{y0} + \sum_{yi=1}^7 (a_{yi}\cos(yi \cdot \omega_y \cdot t) + b_{yi}\sin(yi \cdot \omega_y \cdot t)) \right) y \\
 = F + F_0 \cos(\omega \cdot t) + Mg
 \end{aligned} \tag{17}$$

The differential equation of motion (17) is solved by MATLAB program. When the defect is located at the bottom of the outer raceway of the bearing, its influence on the load distribution, elastic deformation, and contact stress only exists in the vertical direction.³¹ The time domain of the rolling bearing rotor system with defective outer raceway in the vertical direction are mainly analyzed as shown in Figure 8.

When there is defect in the bearing raceway, the vibration amplitude in the vertical direction of the bearing rotor system increases significantly. However, the vibration amplitude of the rotor system gradually decreases and tends to be periodically stable with the change of time. When the rolling element passes through the defect, the contact stress between the rolling element and the bearing raceway, load distribution will change, so the stiffness change period is equal to the rotation time t between the two rolling elements:

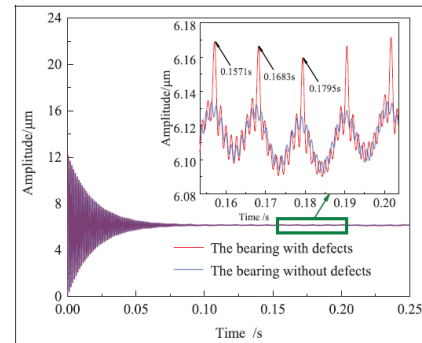


Figure 8. Vertical amplitude of defective bearing rotor system.

$$t = \frac{120D_{pw}}{nZ(D_{pw} - D_w \cos \alpha)} \tag{18}$$

11105

Where α is the bearing contact angle, and the deep groove ball bearing contact angle is 0° . According to formula (18), the stiffness change period of bearing 6206 is 0.0112 s. From Figure 6, the rolling element passes through the bearing raceway

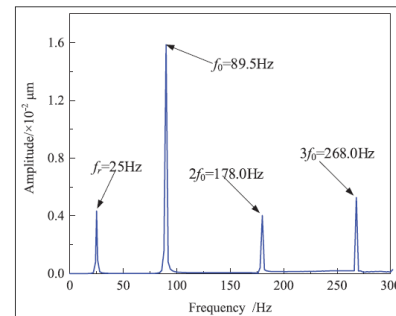


Figure 9. Vertical vibration frequency spectrum of the rolling bearing rotor system with defective raceways.

defect at 0.1571, 0.1683, 0.1795 s, etc., and the vibration amplitude of the rolling bearing rotor system increases instantaneously. This time interval is consistent with the theoretical result from formula (18).

On this basis, the vertical vibration spectrum of the raceway bearing rotor system with raceway defects is analyzed by the fast Fourier transform method. The results are shown in Figure 9. The fault characteristic frequency of rolling bearing outer raceway can be calculated by the following formula³²:

$$f_o = \frac{Zf_r}{2} \left(1 - \frac{D_w}{D_{pw}} \cos \alpha \right) \quad (19)$$

Where f_r is the rotor rotation frequency. The theoretical calculation value of the outer raceway fault characteristic frequency is 89.44 Hz. In Figure 8, the vibration of the rolling bearing rotor system is large at 25, 89.5, 178.0, and 268.0 Hz, which is respectively equal to the rotation frequency of the rotor, the frequency of the outer raceway defects of the bearing, double and triple frequency of outer raceway defect frequency. The corresponding amplitude at the frequency of the bearing outer raceway defect frequency is the largest and most prominent.

Vibration test and result analysis of rolling bearing rotor system

Test system

The test system is shown in Figure 10, including vibration test bench, vibration signal acquisition system, and data processing system. The bearings at both ends of the vibration test bench are the tested bearings, which are all deep groove ball bearings 6206 with defects in the outer raceway (as shown in Figure 11). The relevant performance parameters are shown in Table 1. The test bench loads the bearing rotor system through the loading bearing. The rotor is driven by the motor through the coupling, and the vibration response is tested by four acceleration sensors symmetrically installed in the 45° direction along the radial direction of the rotor at both ends of the bearing pedestal, as shown in Figure 10. The vibration signal of the system is produced by the acceleration sensor, which is amplified by the signal amplifier and then transmitted to the data acquisition card. The output end is connected to the computer and the vibration signal is analyzed and processed by the data processing system. The sampling frequency of vibration signal is 10 kHz, the acceleration sensors are uniaxial piezoelectric sensors. The sensitivity of the

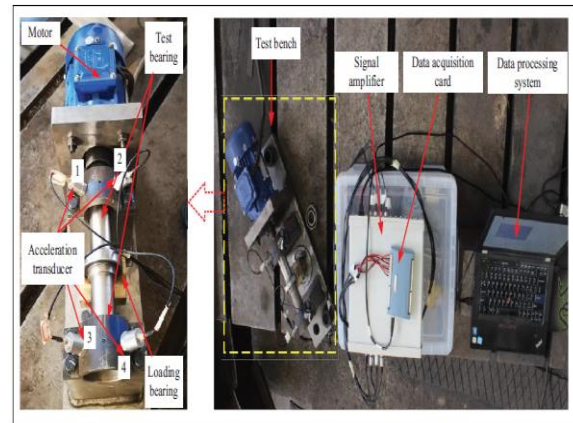


Figure 10. Vibration test bench.

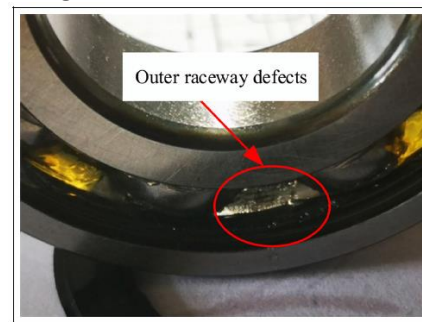


Figure 11. Defective bearing.

sensor is 500 mV/g and range of data acquisition is from 0.2 to 15 kHz.

Test result analysis

As there is a defect on the outer raceway of the rolling bearing, the bearing rotor system shows obvious abnormal vibration. At this time, the vibration signals acquired from the acceleration sensors at the four monitoring points of the test bearing at both ends are shown in Figure 12.

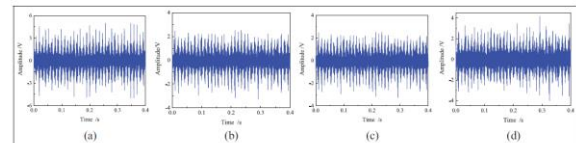


Figure 12. Vibration signal at time domain: (a) monitoring point no. 1, (b) monitoring point no. 2, (c) monitoring point no. 3, and (d) monitoring point no. 4.

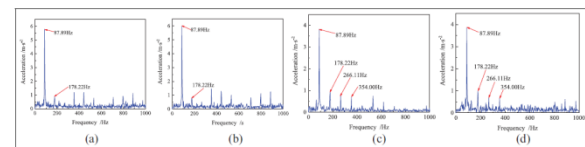


Figure 13. Envelope spectrum of test data: (a) monitoring point no. 1, (b) monitoring point no. 2, (c) monitoring point no. 3, and (d) monitoring point no. 4.

The vibration responses at the four points exist obvious vibration shock, especially the

monitoring points no. 1 and no. 2 of the front-end test bearing. The envelope spectrums of each vibration signal are shown in Figure 13

The envelope spectrum of the vibration signal of monitoring points no. 1 and no. 2 at the front bearing shows that the amplitude of the test bearing is the most obvious at the frequency of 87.89 Hz, which is very close to the fault frequency of 89.44 Hz corresponding to theoretical calculation and numerical analysis. But the theoretical value is still different from the experimental value. The main reason is that the rolling element is not pure rolling in the test, and the friction loss maybe appear because of the sliding of the rolling element. The lubrication of rolling bearing is not the ideal state in the test, the poor lubrication condition will cause the friction loss. Besides, the size, length, and depth of the defect will also lead to a certain change in the vibration frequency in the test.

At the monitoring points no. 3 and no. 4, the envelope spectrum of the vibration signal has the maximum amplitude at 87.89 Hz (as shown in Figure 13), and also has obvious amplitude at its double, triple and quadruple frequency.

Conclusion

(1) Taking the rolling bearing rotor system test bench as the research object, the dynamical model of the rolling bearing rotor system is established. The rolling bearing with radial clearance and outer raceway defects is analyzed, and the time-varying stiffness model of rolling bearing is established. The time-varying stiffness of the bearing in the horizontal and vertical directions is fitted by Fourier series expansion, and the function expressions of each time-varying stiffness are obtained.

(2) The dynamical model of rolling bearing rotor system considering radial clearance and outer raceway defects is solved, and the vibration response time-domain curve of the bearing rotor system is obtained. Due to the outer raceway defects, the vibration response shows obvious shock. The fault frequency of the bearing outer raceway defects can also be

obtained by analyzing the frequency spectrum results of the response.

(3) The vibration test of bearing rotor system with outer raceway defects is carried out. The obvious fault frequency is obtained by the envelope spectrum analysis of vibration signal, which is in good agreement with the theoretical value. The test data verifies the correctness of the stiffness model of bearing and the dynamic model of the bearing rotor system.

Declaration of conflicting interests

The author(s) declared no potential conflicts of interest with respect to the research, authorship, and/or publication of this article.

Funding

The author(s) disclosed receipt of the following financial support for the research, authorship, and/or publication of this article: This work is supported by the National Key R&D Program of China (Grant No. 2018YFB2000505).

References

1. Morales-Espejel GE and Wemekamp AW. An engineering drag losses model for rolling bearings. *ProclMechE, Part J: J Engineering Tribology* 2023; 237: 415–430.
2. Wu PL, He CL, Chang Z, et al. Theoretical calculation models and measurement of friction torque for rolling bearings: state of the art. *J BrazSocMechSciEng* 2022; 44: 24.
3. Chen S, Chen W, Liu J, et al. Development of an aero-static bearing system for roll-to-roll printed electronics. *J MicromechMicroeng* 2018; 28: 065002.
4. Yang R, Zhang Z and Chen Y. Analysis of vibration signals for a ball bearing-rotor system with raceway local defects and rotor eccentricity. *Mech Mach Theory* 2022; 169: 14.
5. Savic B, Urosevic V, Ivkovic N, et al. Implementation of a non-linear regression model in rolling bearing diagnostics. *TehnickiVjesn* 2022; 29: 314–321.
6. Hu G, Chen Y, Cui L, et al. Investigation on modeling and formation mechanism of dynamic rotational error for spindle-rolling bearing system. *ApplSci* 2020; 10: 5753.

7. Stribeck R. Ball bearings for various loads. *Trans ASME* 1907; 29: 420–426.
8. Elastic PH. Elastic Spielschwingungen Konstant Walzger. *Werkstatt und Betrieb* 1950; 3: 354–358.
9. Larizza F, Moazen-Ahmadi A, Howard CQ, et al. The importance of bearing stiffness and load when estimating the size of a defect in a rolling element bearing. *Struct Health Monit* 2019; 18: 1527–1542.
10. Nakhatakyian FG, Puzakina AK and Nakhatakyian DF. The importance of bearing stiffness and load when estimating the size of a defect in a rolling element bearing. *Struct Health Monit* 2022; 49(47): 591–603.
11. Zhang XN, Han QK, Peng ZK, et al. Stability analysis of a rotor-bearing system with time-varying bearing stiffness due to finite number of balls and unbalanced force. *J Sound Vib* 2013; 332: 6768–6784.
12. Li XP, Chen RZ, Shang DY, et al. Dynamic response of maneuvering flight friction rotor with variable stiffness bearing. *J Harbin Inst Technol* 2020; 52: 1–7.
13. Cheng H, Zhang Y, Lu W, et al. Mechanical characteristics and nonlinear dynamic response analysis of rotor-bearing-coupling system. *Appl Math Model* 2021; 93: 708–727.
14. Petersen D, Howard C and Prime Z. Varying stiffness and load distributions in defective ball bearings: analytical formulation and application to defect size estimation. *J Sound Vib* 2015; 337: 284–300.
15. Chen RL, Zhao SD, Zhang MH, et al. Time-varying stiffness model and load-bearing characteristics analysis of angular contact ball bearings. *Mach Des Res* 2022; 38: 114–119.
16. Cao H, Li Y, He Z, et al. Time varying bearing stiffness and vibration response analysis of high speed rolling bearing-rotor systems. *J Mech Eng* 2014; 50: 73–81.
17. Liu Y and Zhang Y. A research on the time-varying stiffness of the ball bearing considering the time-varying number of laden balls and load distribution. *ProclMechE, Part C: J Mechanical Engineering Science* 2019; 233: 4381–4396.
18. Cheng H, Zhang Y, Lu W, et al. Research on time-varying stiffness of bearing based on local defect and varying compliance coupling. *Measurement* 2019; 143: 155–179.
19. Petersen D, Howard C, Sawalhi N, et al. Analysis of bearing stiffness variations, contact forces and vibrations in radially loaded double row rolling element bearings with raceway defects. *Mech Syst Signal Process* 2015; 50–51: 139–160.
20. Cui L, Zhang Y, Zhang F, et al. Vibration response mechanism of faulty outer race rolling element bearings for quantitative analysis. *J Sound Vib* 2016; 364: 67–76.
21. Jiang Y, Huang W, Luo J, et al. An improved dynamic model of defective bearings considering the three-dimensional geometric relationship between the rolling element and defect area. *Mech Syst Signal Process* 2019; 129: 694–716.
22. Singh S, Howard CQ, Hansen CH, et al. Analytical validation of an explicit finite element model of a rolling element bearing with a localised line spall. *J Sound Vib* 2018; 416: 94–110.
23. Zhao Z, Yin X and Wang W. Effect of the raceway defects on the nonlinear dynamic behavior of rolling bearing. *J Mech Sci Technol* 2019; 33: 2511–2525.
24. Tang H, Liu H, Zhao Y, et al. Analysis of mechanics around a localised surface defect of cylindrical roller bearing. *ProclMechE, Part K: J Multi-body Dynamics* 2019; 233: 391–403.
25. Ma Q, Liu Y, Yang S, et al. A coupling model of high-speed train-axle box bearing and the vibration characteristics of bearing with defects under wheel rail excitation. *Machines* 2022; 10: 1024.
26. Lu Z, Wang X, Yue K, et al. Coupling model and vibration simulations of railway vehicles and running gear bearings with multitype defects. *Mech Mach Theory* 2021; 157: 25.
27. Ri C, O R, Zhao Q, et al. Dynamic analysis of the single rotor-bearing system



considering the comprehensive stiffness and damping. *J Mech* 2022; 38: 284–304.

28. Zhu YS, Yuan X, Zhang YY, et al. Vibration modeling of rolling bearings considering compound multi-defect and appraisal with Lempel-Ziv complexity. *J Vib Shock* 2013; 32: 23–29.

29. Kong F, Huang W, Jiang Y, et al. Research on effect of damping variation on vibration response of defective bearings. *AdvMechEng* 2019; 11: 12.

30. Liu ZG, He SQ, Liu H, et al. Rolling bearing application. Beijing: China Machine Press, 2007.

31. Chen RL, Han Q, Zhang MH, et al. Stiffness model of rolling bearing considering clearance and analysis of its time-varying characteristic. *J MechTransm* 2021; 8: 14.

32. Sharma A, Upadhyay N, Kankar PK, et al. Nonlinear dynamic investigations on rolling element bearings: A review. *AdvMechEng* 2018; 10: 15.

33. Rai A and Upadhyay SH. A review on signal processing techniques utilized in the fault diagnosis of rolling element bearings. *TribolInt* 2016; 96: 289–306.

